Science Arts & Métiers (SAM)

is an open access repository that collects the work of Arts et Métiers Institute of Technology researchers and makes it freely available over the web where possible.

This is an author-deposited version published in: https://sam.ensam.eu
Handle ID: .http://hdl.handle.net/10985/21115

To cite this version :

Sébastien JÉGOU, F. GUITTONNEAU, Mihaela TEODORESCU, Laurent BARRALLIER - Influence of oxidizing and Nitriding parameters on nitrogen concentration of electrical steels - Materials Characterization - Vol. 182, p.111529 - 2021

Any correspondence concerning this service should be sent to the repository Administrator : scienceouverte@ensam.eu

Arts et Métiers Institute of Technology

Materials Characterization

Influence of Oxidizing and Nitriding Parameters on Nitrogen Concentration of Electrical Steels

--Manuscript Draft--

Manuscript Number:	MATERIALSCHAR-D-21-01879R1
Article Type:	Review article
Keywords:	Electrical Steel; oxidizing; Nitriding; DIFFUSION; Phase Transformations
Corresponding Author:	Sébastien Jégou Arts et Metiers Institute of Technology Aix-en-Provence, FRANCE
First Author:	Sébastien Jégou
Order of Authors:	Sébastien Jégou
	Mihaela Teodorescu
	Laurent Barrallier
	Fabrice Guittonneau
Abstract:	The influence of oxidizing and nitriding parameters on the nitrogen concentration of grain-oriented electrical steels preliminary to the development of the final Goss texture was explored. Results show that the nitrogen enrichment is driven by a ferrite to austenite transformation during thermochemical treatments. Such a transformation is promoted by (i) a redistribution of ferrite-forming elements close to the surface during oxidizing prior to nitriding, (ii) the oxygen content within the oxide layer prior to nitriding, (iii) the temperature of oxidizing and nitriding, and (iv) the nitrogen enrichment during nitriding. Optimization of the nitrogen content, and thus the precipitation kinetics of alloying elements nitrides (e.g. inhibitors) required for the development of the final Goss texture can be controlled by an optimization of the oxide layer growth, the temperatures and gas mixture of nitriding.
Suggested Reviewers:	Thierry Czerwiec Thierry.czerwiec@univ-lorraine.fr
	Philippe Jacquet philippe.jacquet@ecam.fr
	Luc Pichon luc.pichon@univ-poitiers.fr
	Sebastien Dubent sebastien.dubent@lecnam.net
Response to Reviewers:	

Powered by Editorial Manager® and ProduXion Manager® from Aries Systems Corporation

Highlights

- The nitrided layer of electrical steels is coincident with the oxide layer
- The nitrogen content increases with the decrease of the nitriding temperature
- Oxidizing induces a redistribution of heavy elements (Si, Cr, Mn, Al)
- The nitrogen enrichment is driven by a ferrite to austenite transformation
- The austenite transformation is promoted by diffusing Si, O and N

Manuscript File Click here to view linked References

Influence of Oxidizing and Nitriding Parameters on Nitrogen Concentration of Electrical Steels

S. Jégou[1], M. Teodorescu[2], L. Barrallier[1], F. Guittonneau[1]

[1] Arts et Metiers Institute of Technology, MSMP, HESAM Université, F-13617 Aix-en-Provence, France
[2] thyssenkrupp Electrical Steel UGO, Isbergues, France

sebastien.jegou@ensam.eu, Mihaela.Teodorescu@thyssenkrupp.com, laurent.barralier@ensam.eu, fabrice.guittonneau@ensam.eu

Corresponding author: S.Jégou, sebastien.jegou@ensam.eu, Arts et Metiers Institute of Technology, MSMP, HESAM Université, F-13617 Aix-en-Provence, France

Abstract

The influence of oxidizing and nitriding parameters on the nitrogen concentration of grain-oriented electrical steels preliminary to the development of the final Goss texture was explored. Results show that the nitrogen enrichment is driven by a ferrite to austenite transformation during thermochemical treatments. Such a transformation is promoted by (i) a redistribution of ferrite-forming elements close to the surface during oxidizing prior to nitriding, (ii) the oxygen content within the oxide layer prior to nitriding, (iii) the temperature of oxidizing and nitriding, and (iv) the nitrogen enrichment during nitriding. Optimization of the nitrogen content, and thus the precipitation kinetics of alloying elements nitrides (e.g. inhibitors) required for the development of the final Goss texture can be controlled by an optimization of the oxide layer growth, the temperatures and gas mixture of nitriding.

Keywords

Electrical steel, oxidizing, nitriding, diffusion, phase transformations

1. Introduction

The evolution of environmental concerns in the last decay has been pushing electrical conversion systems to new developments and challenging optimizations. In case of electrical transformers, a complex process route leads to decrease core lost and increase the magnetic permeability [1-3]. A succession of hot and cold rolling, thermochemical surface and heat treatments have been optimized to manufacture so called “grain-oriented” (GO) electrical steels. The quality of the final crystallographic texture, e.g. Goss texture, directly drives the electrical performances. Goss texture, {110}<001>, develops due to an abnormal grain growth thanks to, at least, the presence of grain-growth inhibitors within the microstructure such as MnS precipitates and alloying elements nitrides MN (M = Si, Al,

Cr…) [4-8]. Optimizing such a complex process route appears time consuming, costly and complex, especially because the magnetic properties can only be measured when the entire process route was accomplished.

In case of MN inhibitors, three nitriding treatments have been optimized to promote such a precipitation: (i) inherent nitriding from nitrogen available in the materials from casting [5], (ii) equilibrium nitriding from reaction of dinitrogen N_2 during the last heat treatment during which the Goss texture develops [10-11] and (iii) non-equilibrium nitriding from reaction of ammonia NH_3 in-line after the oxidizing treatment [8-9]. Inherent and equilibrium nitriding do not promote a high enough adsorption of nitrogen by the steel, leading to non-optimized fraction of inhibitors to promote the Goss texture [9]. Development of the non-equilibrium nitriding treatment regarding the magnetic properties has been reached identifying the acceptable range of nitrogen concentration for an efficient abnormal grain growth, the corresponding temperature of nitriding, and the range of ammonia to dihydrogen ratio to use in order to get satisfying precipitation of inhibitors [12-13]. Prior to nitriding, oxidizing aims decarburizing electrical steels as well as the later growth of an insulated layer (glass film) [14-16]. Studies were carried out on the structure of the oxides' layer and on influence of process parameters on oxides' layer properties. [17-18]. However, details about the nitriding kinetics, and most of all on the influence of the oxide layer on nitriding kinetics, and thus on the nitrogen enrichment and on control of the precipitation of inhibitors are missing in the literature [19-25].

The present work aims to study the influence of oxidizing and nitriding parameters on the nitrogen adsorption and diffusion kinetics right before the development of the final Goss texture.

2. Experimental

2.1. Materials

The material is a silicon iron-based alloy used for grain-oriented electrical steel.

Samples of 30x30x0.2 mm^3 were provided by thyssenkrupp Electrical Steel for investigations. Sensitive analysis of annealing parameters was performed through laboratory trails and experimental measurements. Conditions of oxidizing are chosen to promote both oxidizing and decarburizing in a single step. The dew point (T_{DP} controlled by H_2O vapour and a chilled mirror hygrometer) and temperature (T_O) of oxidizing prior to nitriding stage were varied from 40 to 70°C and from 840°C to 900°C respectively. Samples have then been nitrided in a gas mixture using H_2, N_2 and NH_3, at various temperatures (T_N), from 770°C to 930°C. The nitriding potential (defined by the fraction of both NH_3 and H_2) was kept fixed to a usual low value used for electrical steels according to industrial practice because of the complexity to control low nitriding potential in industrial conditions especially at such high temperature (higher than 600 °C). Cases without nitriding were as well considered in order to dissociate the various parameters influences. The studied GO samples had the following main chemical composition 3.1 wt.% Si, 0.028 wt.%Al, 0.15 wt.% Mn, 0.0095 wt.% N and almost no C, the samples being already decarburised before the experimental measurements.

2.2. Materials characterization

The microstructure was observed by scanning electron microscopy (SEM) using a Jeol JSM-7001F microscope and backscatter electrons mode. Prior to observations, ionic polishing (Ar+ ions, 4 kV) was performed on each transversal cut using a Jeol Cross Section Polisher.

Chemical analysis was carried out by glow discharge optical emission spectroscopy (GDOES) using a Profiler 2 device from Horiba. The surface of interest was around 4 mm in diameter parallel to the surface of the sheet. The RF power, gas pressure and time of analysis were set to 35 W, 680 Pa and 300 s respectively, that corresponds to a depth of erosion of approximatively 15 µm. Errors on chemical analysis are expected to be less than 10 %, and were less than 2 and 1 % for nitrogen and silicon respectively on a standard.

X-ray diffraction phase analyses were performed at room temperature using a Siemens D500 diffractometer, an Elphyse linear detector and the chromium $K\alpha$ radiation. The diffraction angle 2θ was varied from 40 to 140°, that corresponds to a penetration depth of 2 to 6 µm in the ferritic matrix.

2.3. Thermodynamics calculations

Thermodynamics calculations were performed using Thermo-Calc version 2021a, TCFE Steels/Fe-alloys database version 07 and TC-Python [26].

3. Results

3.1. Microstructure observation

Figure 1 shows an example of the microstructure after oxidizing and nitriding observed by SEM using the backscattered electron mode. The outer surface is characterized by an oxide layer of approximatively 2 µm thickness. The oxide layer is divided in two sublayers, one subscale at the extreme surface of nearly 0.5 µm thickness composed of Fe_2SiO_4 and FeO oxides and one of approximatively 1.5 µm composed of globular followed by lamellar SiO_2 oxides [27]. All the samples present similar type of composition, but their distribution, volume fraction and inner properties could be different depending on the process parameters. The detailed analysis of the oxides' layer components and their properties is not the main focus of this paper, the related results will be part of another paper.

3.2. Chemical analysis

Oxygen and nitrogen in-depth profiles were obtained from GDOES analysis. Figure 2 gives a comparison of contents prior to thermochemical treatments, after oxidizing, and with and without gas nitriding. The effective depth of oxygen diffusion is approximatively 2.5 µm. The oxygen content is

maximum at the extreme surface and then decreases, following an internal oxidation diffusion behaviour, to reach a null concentration at 2.5 µm below the surface in agreement with the SEM observations given on Figure 1 for this particular case. The diffusion of nitrogen atoms tends to make the diffusion process of oxygen atoms to continue during nitriding. The nitrogen content in-depth profile exhibits a non-obvious evolution as a function of the depth. It is maximum at the extreme surface, decreases to a minimum of nearly 0.65 wt.% at a depth of 0.5 µm, increases up to 0.8 wt.% at 1.0 µm depth before abruptly decreasing toward the core content (below 0.03 wt.% according to the sensitivity of present GDOES analysis). The effective diffusion depth of nitrogen atoms is in agreements with the one of oxygen. The nitrogen content in the oxide layer highly overestimates the content within the final product that gives a good secondary recrystallization [12].

The affected depth by oxygen atoms increases when the dew point (T_{DP}) and oxidizing (T_O) temperature increase (Figures 3 and 4). The evolution of the content of oxygen as a function of the depth are all similar, characterized by a maximum fraction close to the extreme surface that decreases to a null content within the core. As previously, nitrogen atoms are largely located through the entire oxide layer. The higher the temperature, the lower and deeper the nitrogen enrichment is, and, the lower and deeper the minimum content of nitrogen is. It reaches 0.45 and 0.35 wt.% at a depth of 0.65 µm for a dew point and oxidizing temperatures of 70 and 900 °C respectively (Figure 3.b and 4.b). For low dew point (40 °C), no variation of nitrogen content is observed within the oxide layer. In contrast, a significant decrease of the nitrogen enrichment is noted when the oxidizing temperature is increasing from 840 to 900 °C.

Figure 5 shows the influence of the nitriding temperature (T_N) on the case depth. No significant change is observed in case of the oxide layer growth. The evolution of the nitrogen content shows similar profiles for all temperatures with a minimum of the nitrogen fraction at a depth of nearly 0.5 µm below the surface. However, increasing the nitriding temperature involves a significant decrease of the nitrogen enrichment through the oxide layer. The fraction of nitrogen reaches almost 2.0 wt.% at 770 °C whereas 0.5 wt.% are barely achieved at 930 °C.

By considering the GDOES detection limit of nitrogen atoms (0.03 wt.%), a diffusion zone of nitrogen in α-Fe ferrite below the oxide layer is observed to a depth of 12 µm. All the diffusion zones look similar below the oxide layer with a nitrogen fraction ranging from 0.05 down to 0.03 wt.% except at the low nitriding temperature of 770 °C in case of which the nitrogen fraction ranges from 0.075 down to 0.03 wt.% (Figure 5.b).

One objective of oxidizing prior to nitriding is to decarburize the sample in order to achieve a minimum content required to maximize the abnormal secondary recrystallisation. Figure 6 gives examples of the carbon content in-depth profiles. It is observed that the decarburization of the core material is effective (0.04 down to 0.02 wt.%) whereas it induces a non-negligible enrichment of carbon in the oxide layer for all samples. According to the affected depth, such enrichment may be attributed to the presence of $(Fe,Mn)_2SiO_4$ and FeO close to the surface in the oxide layer (Figure 1).

Despite the GDOES detection limit of carbon (from 0.003 to 0.01 wt.%), these measurements must be considered with precautions because of possible pollution of the surface due to cleaning for instance. More investigations are required to address the carbon enrichment of the oxide layer during oxidizing.

The chemical composition of some alloying elements is given on Figure 7 and 8 as a function of the depth below the surface and the temperatures of oxidizing and nitriding respectively. The same complex tendency as a function of the depth below the surface is observed for all elements. All elements are characterized by a depletion close to the outer surface, an increase of the content followed by a depletion at greater depth. The redistribution of alloying elements is observed at more profound depth when the thickness on the oxide layer increases (Figures 3 and 4). The silicon content is almost constant within the oxide layer and higher than in the core, but some profile variations are noted mostly induced by the change in dew point. Such redistribution of alloying elements through the oxidized surface is at least influenced by the oxidizing treatments (Figure 7) and nitriding does not modify them (Figure 8).

Finally, the total nitrogen uptake into the oxide layer can significantly vary by a factor 4 when increasing the nitriding temperature from 770 to 930 °C (Figure 5) whereas no significant change in the redistribution of carbon nor heavy elements is observed (Figures 6 and 8).

3.3. X-ray diffraction

Figure 9 gives the phase analyses carried out at the surface of samples as a function of the nitriding temperature, as well as after decarburizing. Austenite is identified after nitriding but not present prior to nitriding, or in a too low volume fraction or crystallite size. The lower the nitriding temperature, the higher the volume fraction of austenite is. To complement these results, a tempering was performed, subsequent to nitriding, for one minute at the nitriding temperatures tested previously and followed by water quenching. The tempered samples confirm the presence of retained austenite at room temperature after nitriding.

3.4. Thermodynamic calculations

Figure 10 gives the Fe-Si-N-2.0wt.%O isopleth diagrams at 750 and 950 °C and possible phase transformations at a depth of nearly 0.1 µm. Results show that a ferrite to austenite transformation may occur during oxidizing and nitriding. It is due to the depletion of silicon but also to the enrichment of both oxygen and nitrogen. As a consequence, the transformation is expected to be promoted close to the outer surface according to GDOES analysis. Moreover the transformation is thermally activated enabling the presence of austenite for higher Si content and thus deeper within the oxide layer.

Figure 11 gives the thermodynamic calculations as a function of the chemical composition of samples after nitriding at three different temperatures as measured by GDOES. Results show that austenite is present in the oxy-nitrided layer as deep as 1.0 µm. At 770 °C, the nitrogen enrichment significantly

stabilizes the austenitic phase as compared to without nitriding at the same temperature between 0.2 and 1.0 µm in depth (Figure 11.c).

The fraction of silicon nitrides within the oxi-nitrided layer increases when the temperature of nitriding decreases and must be related to an increase of the nitrogen uptake.

The fraction of oxides does not depend on the nitrogen content and stay nearly unchanged when comparing samples with and without nitriding. In addition, all calculations show that the nature of the silicon oxide may change according to the temperature of both oxidizing and nitriding. Below 850 °C, silicon oxides are quartz like but change to tridymite at higher temperature.

4. Discussion

Chemical characterizations of a GO electrical steel after oxidizing and nitriding show that the kinetics of nitrogen adsorption and diffusion highly depends on the oxide layer growth, on the oxygen and carbon content, on the complex redistribution of heavy elements (such as Si, Cr, Al, Mn), as well as on the temperature of the heat treatments. The nitrogen content in-depth profile exhibits a non-obvious evolution as a function of the depth, with a minimum of nitrogen within the oxide layer.

The higher the temperatures of oxidizing and nitriding, the deeper the diffusion of nitrogen and the lower the maximum of nitrogen in the oxide layer are (Figures 4 and 5 respectively). Nitrogen diffusion is characterized, as mentioned, by a minimum fraction of nitrogen within the oxide layer (close to a depth of 0.5 µm), that is even more pronounced when the oxide layer is thick. The nitrogen uptake does not appear depending in first approximation on the fraction and redistribution of elements such as silicon, chromium, aluminium or manganese (Figures 7 and 8). However this observation reflects the fact that, prior to nitriding, a similar redistribution of elements between oxides and matrix is obtained, for the range of the variations of the decarburizing (oxidizing) temperature considered. But any change in the silicon or aluminium redistribution between the matrix and oxides during oxidizing is obviously expected to play a role on the formation of silicon and aluminium nitrides and thus on the level of the nitrogen uptake during nitriding.

Chemical analyses revealed that oxidizing leads to a decrease of the carbon content within the core material thanks to the decarburizing atmosphere during oxidizing, but results in a carbon enrichment of the oxide layer prior to nitriding (Figure 6). Heavy elements also exhibit a complex redistribution through the oxide layer prior to nitriding (Figures 7 and 8), consistent with the literature using the same chemical analysis method [27]. These redistributions of already present elements are influenced by the conditions of oxidizing and not affected by those of nitriding.

Thermodynamic calculations of temperature isopleths for given oxygen content or using compositions as measured by GDOES show that a ferrite to austenite transformation may occur within the oxide layer during nitriding (Figure 10). The higher the oxygen content and temperature, the lower the transformation point from ferrite to austenite is during nitriding. The ferrite to austenite transformation is as a consequence promoted close to the surface in the oxide layer. Although the carbon fraction

measurement may need optimization for GDOES analysis, the presence of carbon content within the oxide layer can promote such an austenitic transformation. Calculations confirm the present experimental observations of retained austenite by XRD at the surface of samples (Figure 9). Austenite was also observed experimentally at the extreme surface of the oxide layer in other recent works [16, 25]. The fraction of austenite increases in agreement with the nitrogen content according to GDOES analysis and the Fe-N phase diagram [28]. Iron nitrides being more thermodynamically stable than austenite at room temperature [28], tempering after nitriding must promote the decomposition of austenite into ferrite and iron nitrides. It thus leads to no observation of austenite at room temperature by XRD. However iron nitrides were not observed by XRD that suggests a low fraction of iron nitrides or too small crystallites. More investigations are required.

The observation of a minimum of the nitrogen fraction in the oxide layer close to 0.5 µm below the surface is in agreement with the transformation zone from ferrite to austenite according to thermodynamic calculations (Figure 11).

The thermodynamic calculations let us assume that the austenitic transformation can be in competition with the precipitation of silicon nitrides, and so, even more when the transformation point is low (Figure 10). Although the nitrogen solubility limit in austenite is much higher than in ferrite, the precipitation kinetics of alloying elements as nitrides, and so the nitrogen uptake, may be assumed slower if the austenitic transformation occurs before the complete precipitation of nitrides. Moreover, it has to be considered that the diffusion kinetics of nitrogen atoms in austenite is at least one hundred times lower than in a ferritic matrix [29]. It thus leads to a decrease of the flow of nitrogen atoms at the beginning of the oxide layer whereas the diffusion kinetics are much faster in the ferritic area at greater depth.

As a consequence, the calculated gradient of austenite close to the surface is expected to result in a depletion of nitrogen between the low diffusion kinetic area near the surface and the fast diffusion kinetics area (ferrite zone) deeper in the oxide layer. The nitrogen enrichment being slower due to the austenitic transformation prior to the complete precipitation of silicon nitrides at the surface, the boundary conditions for diffusion in the ferritic zone deeper in the material must also change towards lower value. Therefore, it induces a lower level of nitrogen in ferrite and a slower precipitation kinetics of alloying elements as nitrides deeper in the oxide layer.

According to thermodynamic calculations and the higher chemical affinity of both silicon and aluminium with oxygen than nitrogen [30], the oxides already present before nitriding are supposed not to take part in the precipitation of silicon and aluminium nitrides.

Calculations show that the nature of silicon oxides could also change during nitriding function of the content of both oxygen and silicon, but also depending on the temperature of oxidizing and nitriding. Similarly, the nature and fraction of iron-silicon oxide at the outer surface (e.g. $(Fe,Mn)_2SiO4$ and/or FeO) may play a role on the catalytic dissociation of ammonia and the nitrogen adsorption and uptake.

However present experimental results cannot conclude on any effect of such change of oxides on the diffusion kinetics of nitrogen atoms during nitriding.

Finally, it is well known that the natural dissociation rate of ammonia NH_3 into N_2 and H_2 gas mixture increases exponentially with the temperature [31]. As a result, and considering perfect gas transfer to the solid surface, the nitrogen fraction at the gas-solid interface available for adsorption into the solid from the catalytic dissociation of ammonia at the solid surface naturally decreases and thus the nitrogen enrichment within the oxide layer. Moreover, at the atmospheric pressure, the dissociation rate of dinitrogen molecules N_2 during nitriding cannot compensate the lack of nitrogen atoms from the catalytic ammonia dissociation at the solid surface without increasing the pressure [31-33].

5. Conclusion

Influences of the conditions of oxidizing and nitriding on the nitrogen enrichment prior to the development of the final Goss texture were explored in case of a grain-oriented electrical steel. The nitrogen enrichment in the oxide layer can significantly overestimate the nitrogen content required for the development of the final Goss texture. The nitrogen atoms are exclusively located within the about 2.5 µm thick oxide layer after nitriding. The nitrogen diffusion kinetics through the oxide layer depends on a ferrite to austenite transformation during oxidizing and nitriding. The transformation point decreases with (i) the increase of the fraction of oxygen, carbon and nitrogen atoms, (ii) the depletion of heavy elements very close to the outer surface and (iii) the temperature increase.

The nitrogen content, that leads to the optimized precipitation of inhibitors required for the development of the final Goss texture and the optimum magnetic properties, is driven by the oxidizing and nitriding conditions that must be involving a ferrite to austenite transformation if not controlled. The nitrogen enrichment, and thus the development of inhibitors, can obviously be optimized and controlled depending on the conditions of oxidizing and nitriding. It arises that optimize the nitriding potential through the gas mixture (NH_3-N_2-H_2) could also be necessary in order to get the most efficient thermochemical treatments conditions of electrical steels.

Data availability

The raw/processed data required to reproduce these findings cannot be shared at this time as the data also forms part of an ongoing study

References

[1] Littmann M.F., Iron and Silicon-Iron Alloy, IEEE Transactions on Magnetics MAG-7(1) (1971) 48-69

[2] Taguchi S., Sakakura A., Matsumoto F., Takashima K., Kuroki K., The development of grain-oriented silicon steel with high permeability, Journal of Magnetism and Magnetic Materials 2 (1976) 121-131

[3] Ushigami Y., Masui H., Okazaki Y., Suga Y., Takahashi N., Development of low-loss grain-oriented silicon steel, Journal of Materials Engineering and Performance 5(3) (1996) 310-315

[4] Markuszewicz M., Groyecki J., Lassota J., Zawada A., Stability of inclusions and the formation of secondary grains in silicon-iron alloys, Transactions of the Metallurgical Society of AIME 236 (1966) 196-200

[5] Fiedler H., A comparison of the use of aluminum and vanadium nitrides for making grain-oriented silicon-iron, Journal of Applied Physics 38(3) (1967) 1098-1099

[6] Matsuoka T., Effect of impurities on the development of (110)[001] secondary recrystallization texture in 3% silicon iron, Transactions ISIJ 7 (1967) 19-28

[7] Grenoble H.E., The role of solutes in the secondary recrystallization of silicon iron, IEEE Transactions on Magnetics MAG-13(5) (1977) 1427-1432

[8] Ushigami Y., Nakayama T., Suga Y., Takahashi N., Influence of inhibitor intensity on secondary recrystallization in Fe-3%Si alloy, Materials Science Forum 204-206 (1996) 599-604

[9] Takahashi N., Harase J., Recent development of technology of grain oriented silicon steel, Materials Science Forum 204-206 (1996) 143-154

[10] Suga Y., Matsumoto F., Nakayama T., Japanese Patent, Application No.S57-165066 (1982)

[11] Konno T., Suga Y., Nakamura M., Komatsu H., Japanese Patent, Application No.S59-215827 (1984)

[12] Kobayashi H., Kuroki K., Minakuchi M., Yakashiro K., United States Patent 4,979,996 (1990)

[13] Ushigami Y., Nakayama T., Suga Y., Takahashi N., Influence of secondary recrystallization temperature on secondary recrystallization texture in Fe-3%Si alloy, Materials Science Forum 204-206 (1996) 605-610

[14] Yamazaki T., On the decarburization of silicon steel sheet, Transactions ISIJ 9 (1969) 66-75

[15] Block W.F., Jayaraman N., Reactions during decarburization annealing of electrical steel, Materials Science and Technology 2 (1986) 22-27

[16] Wu X-l., Li X., Yang P., Jia Zh-w., Zhang H-l., Analysis of oxide layer structure in nitrided grain-oriented silicone steel, International Journal of Minerals, Metallurgy and Materials, 26(12) (2019) 1531-1538

[17] Lyudkovsky G., Preban A.G., Shapiro J.M., The influence of annealing conditions on the internal oxidation and magnetic properties of silicon-aluminium bearing electrical steels, Journal of Applied Physics 53(3) (1982) 2419-2421

[18] Cesar M.G.M.M., Mantel M.J., Effect of the temperature and dew point of the decarburization process on the oxide subscale of a 3% silicon steel, Journal of Magnetism and Magnetic Materials 254-255 (2003) 337-339

[19] Kumano T., Haratani T., Fujii N., Effect of nitriding on grain-oriented steel bearing aluminium, ISIJ International 45(1) (2005) 95-100

[20] Kumano T., Ohata Y., Fujii N., Ushigami Y., Takeshita T., Effect of nitriding on grain-oriented steel bearing aluminium (the second study), Journal of Magnetism and Magnetic Materials 304 (2006) e602-e607

[21] Liao Ch-Ch., Hou Ch-K., Effect of nitriding time on secondary recrystallization behaviors and magnetic properties of grain-oriented electrical steel, Journal of Magnetism Materials 322 (2010) 434-442

[22] Zeng G., Luo H., Li J., Gong J., Li X., Wang X., Experimental studies and numerical simulation on the nitriding process of grain-oriented silicon steel, Acta Metallurgica Sinica 53(6) (2017) 743-750

[23] Wen P., Luo H., Zeng G., Li J., Huang J., Yan B., In-situ measurement and numerical simulation of nitriding kinetics of grain-oriented silicon steel, International Journal of Hydrogen Energy 42 (2017) 10901-10910

[24] Vilela T.J.S., Faria Fonseca A.J., Costa Paolinelli S., Barros Cota A., Simultaneous decarburizing and nitriding : effects on structure and magnetic properties of 3% Si grain-oriented electrical steel, REM, International Engineering Journal 71(4) (2018) 599-604

[25] Guo Q., Li X., Gong P., Nutter J., Rainforth W.M., Luo H., Why does nitriding of grain-oriented silicon steel become slower at higher temperature? Steel Research International (2021) 2000545

[26] Andersson J.O., Helander T., Höglund L., Shi P.F., and Sundman B., Thermo-Calc and DICTRA, Computational tools for materials science, Calphad, 26 (2002) 273-312

[27] Sehoon Jung, Min Serk Kwon, Seung Bin Kim, Kwang Soo Shin, Characterization of chemical information and morphology for in-depth oxide layers in decarburized electrical steel with glow discharge sputtering, Surf. Interface Anal. 45 (2013) 1119-1128

[28] Wriedt H.A., Gokcen N.A., Nafziger R.H., The Fe-N (Iron-Nitrogen) System, Bulletin of Alloy Phase Diagrams 8(4) (1987) 355-377

[29] Fast J.D., Verrijp M.B., Diffusion of nitrogen in iron, Journal of the Iron and Steel Institute 176 (1954) 24-27

[30] P.J. Linstrom and W.G. Mallard, Eds., NIST Chemistry WebBook, NIST Standard Reference Database Number 69**,** National Institute of Standards and Technology, Gaithersburg MD, 20899, https://doi.org/10.18434/T4D303

[31] Schulz G., Schaefer H., Untersuchung der Bildungsgleichgewichte des Ammoniaks und Trideuteroammoniaks, Berichte der Bunsengesellschaft für physikalische Chemie 70(1) (1966) 21-27

[32] Grabke H.J., Reaktionen von Ammoniak, Stickstoff und Wasserstoff an der Oberfläche von Eisen I. Zur Kinetik der Nitrierung von Eisen mit NH_3- H_2- Gemischen und der Denitrierung, Berichte der Bunsengesellschaft für physikalische Chemie 72(4) (1968) 533-541

[33] Grabke H.J., Reaktion von Ammoniak, Stickstoff und Wasserstoff an der Oberfläche von Eisen II. Zur Kinetik der Nitrierung von Eisen mit N_2 und der Desorption von N_2, Berichte der Bunsengesellschaft für physikalische Chemie 72(4) (1968) 541-548

Figure Click here to access/download;Figure;Article_v09_Figures.docx

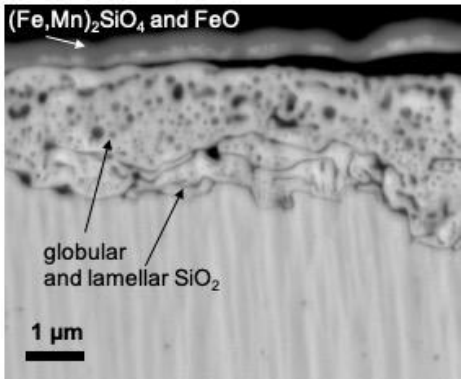

Figure 1: SEM micrography in backscattered mode of a GO electrical steel after oxidizing (T_{DP} = 60 °C, T_O = 870 °C) and nitriding (T_N = 880 °C).

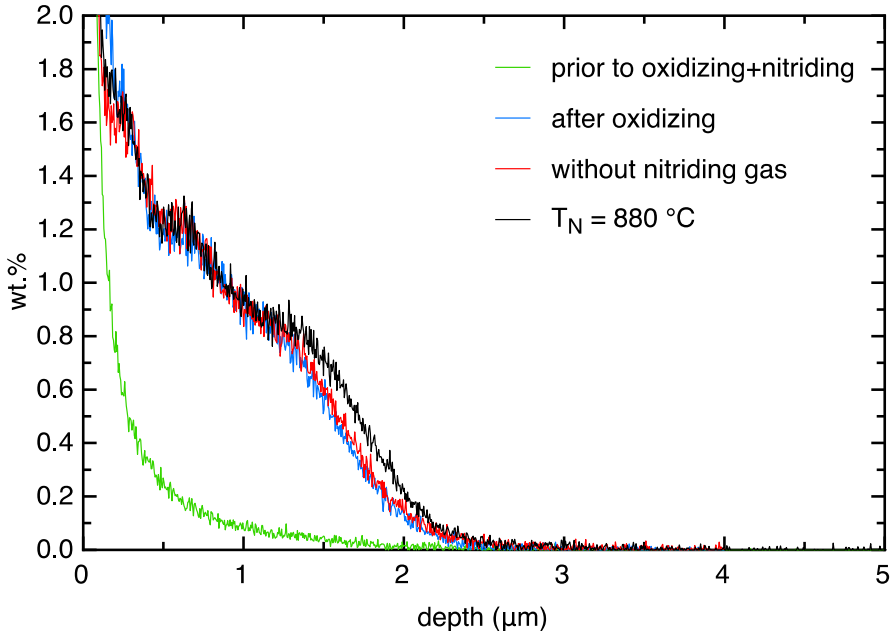

a. Oxygen

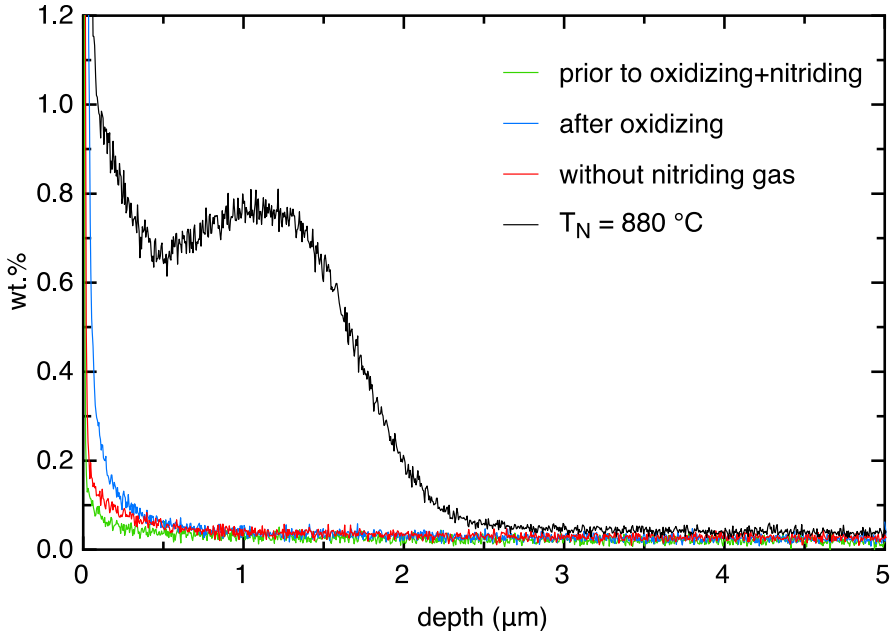

b. Nitrogen

Figure 2: GDOES chemical analyses of GO electrical steel prior to oxidizing and nitriding, after oxidizing, and with and without gas nitriding. (a) oxygen and (b) nitrogen in-depth content profiles.

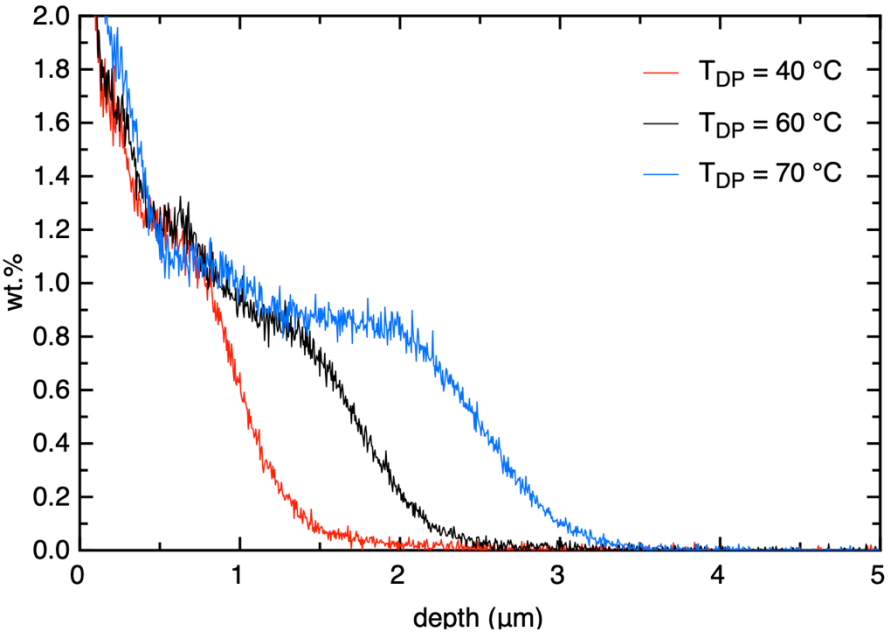

a. Oxygen

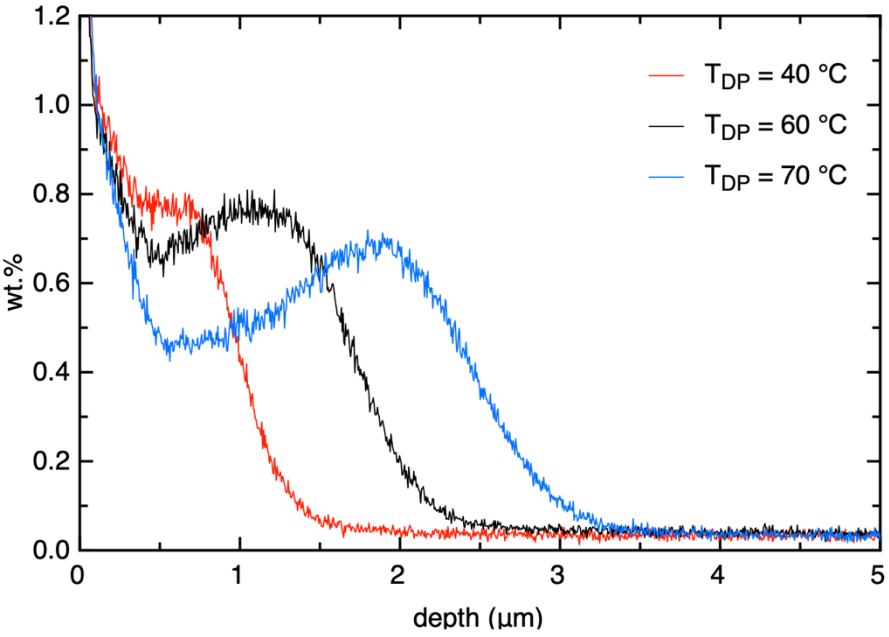

b. Nitrogen

Figure 3: GDOES chemical analyses of GO electrical steel. Influence of the dew point (T_{DP}) of oxidizing on (a) oxygen and (b) nitrogen in-depth content profiles.

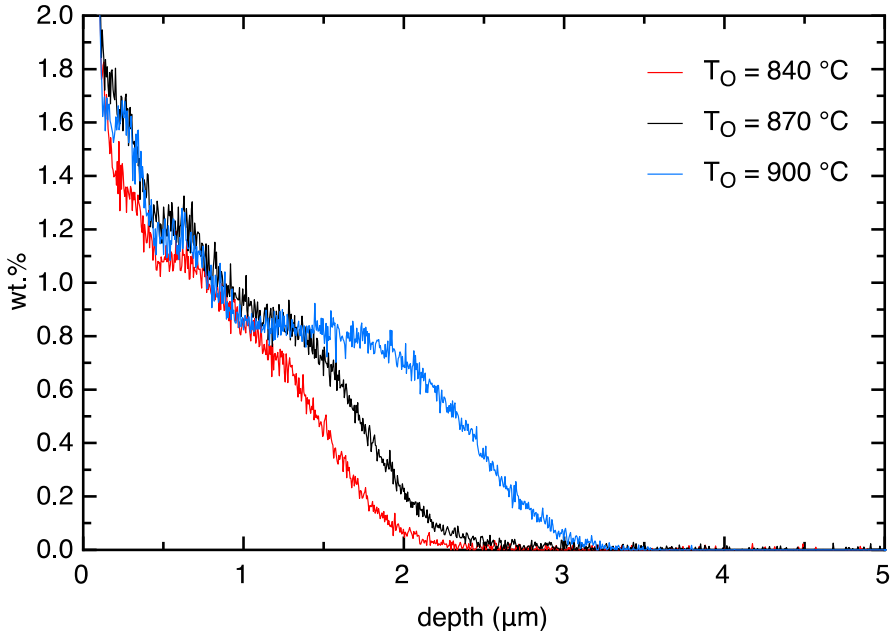

a. Oxygen

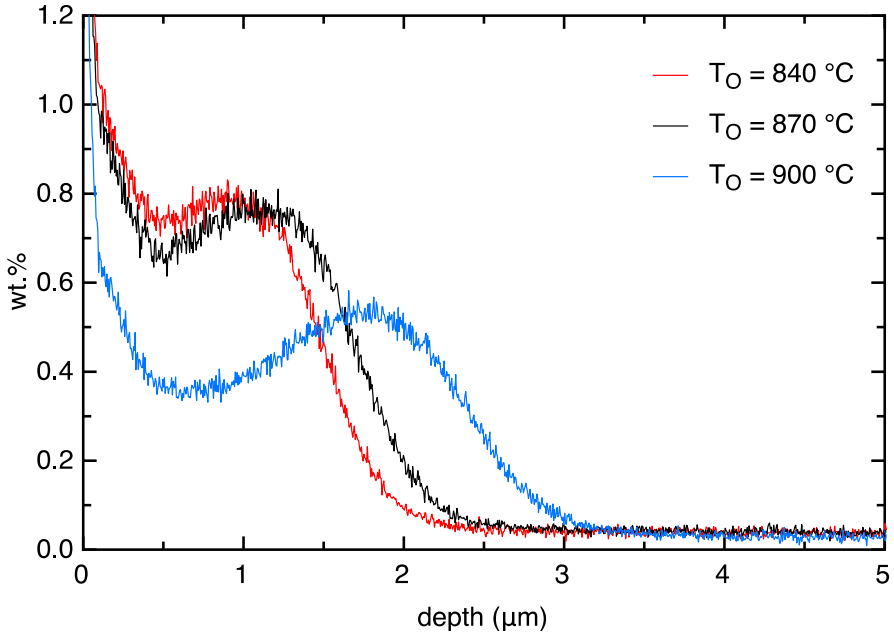

b. Nitrogen

Figure 4: GDOES chemical analyses of GO electrical steel. Influence of the oxidizing temperature (*To*) on (a) oxygen and (b) nitrogen in-depth content profiles.

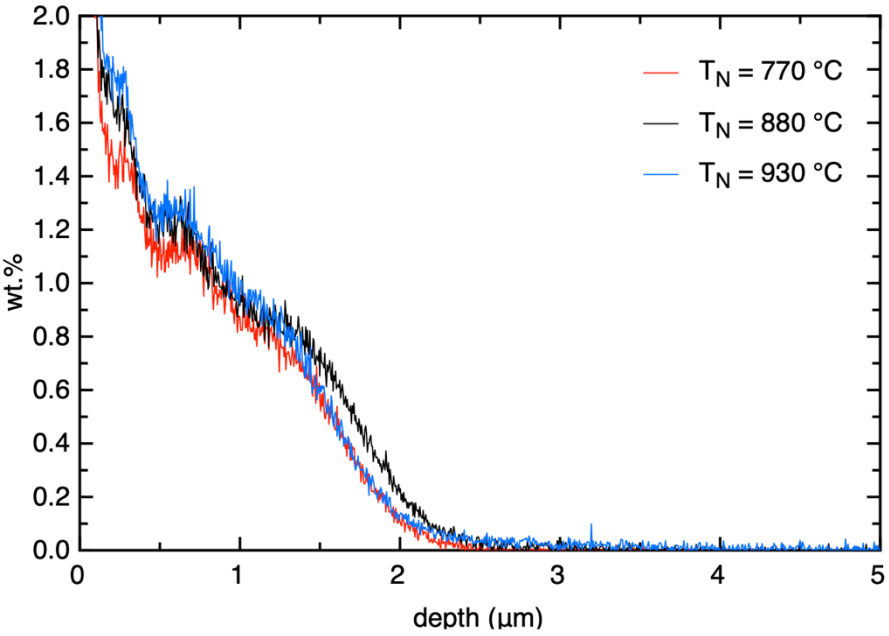

a. Oxygen

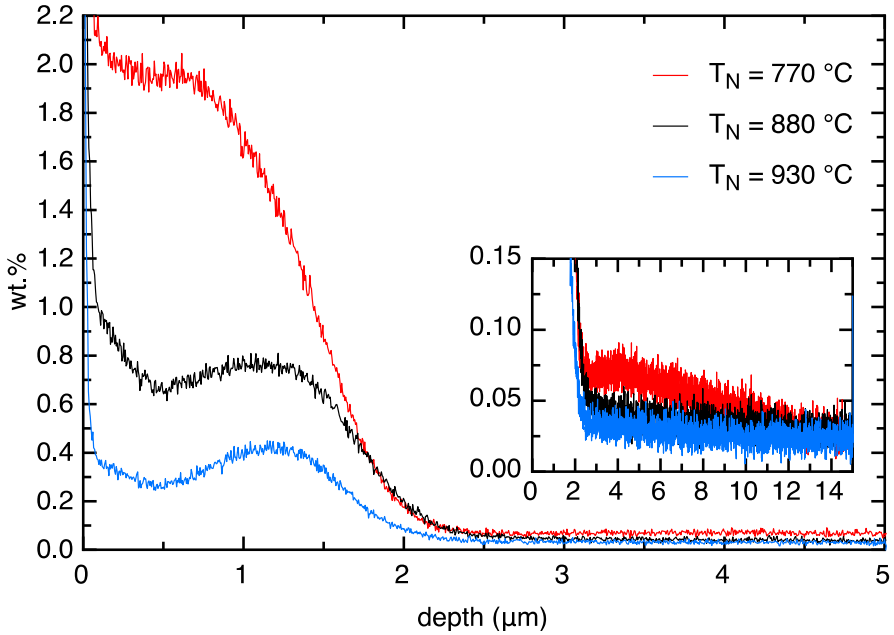

b. Nitrogen

Figure 5: GDOES chemical analyses of GO electrical steel. Influence of the nitriding temperature (T_N) on (a) oxygen and (b) nitrogen in-depth content profiles.

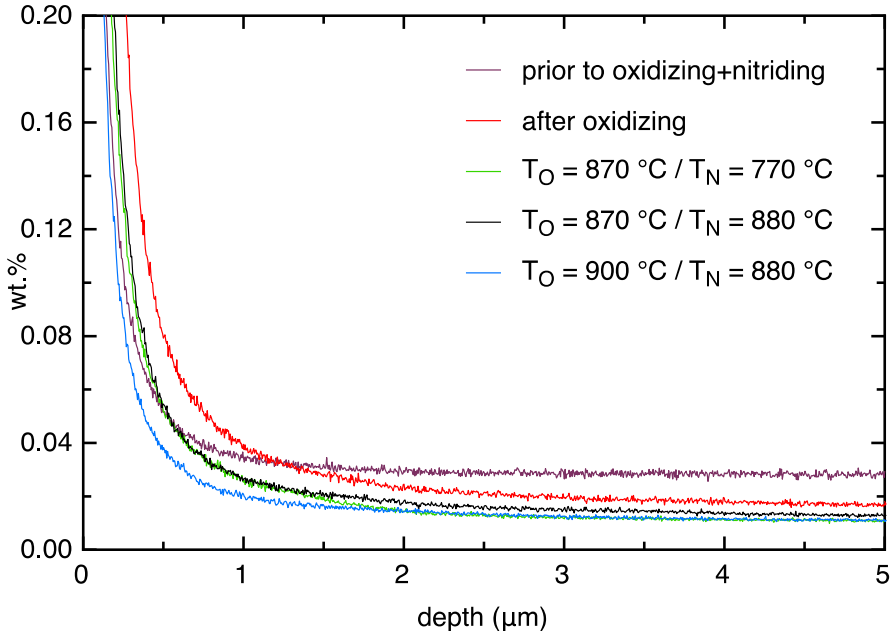

Figure 6: Carbon in-depth profiles from GDOES chemical analyses of GO electrical steel. Comparison of the carbon content at different steps of thermochemical treatments and influence of the temperature of oxidizing (T_O) and nitriding (T_N).

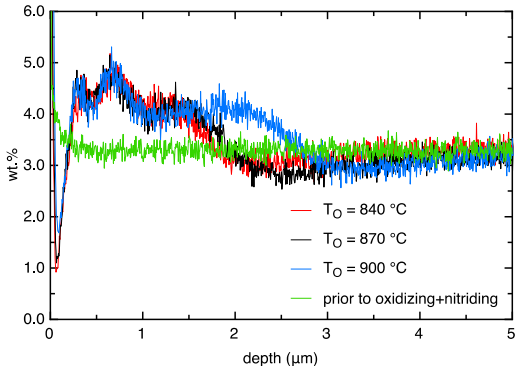

a. Silicon

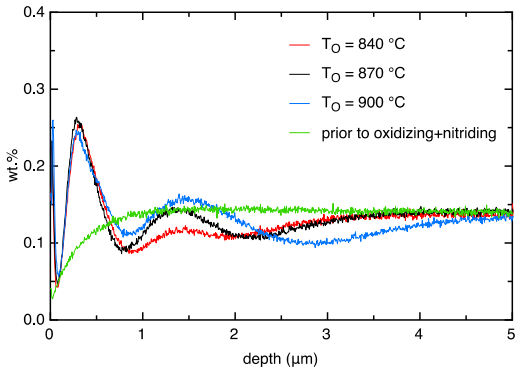

b. Chromium

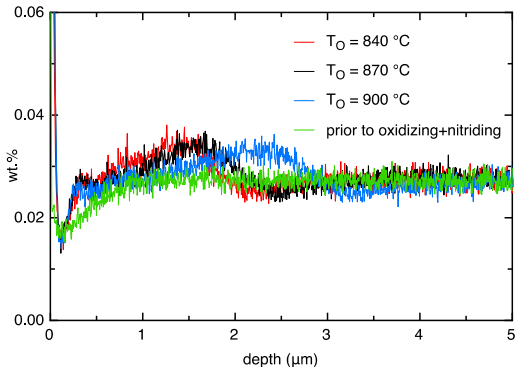

c. Aluminium

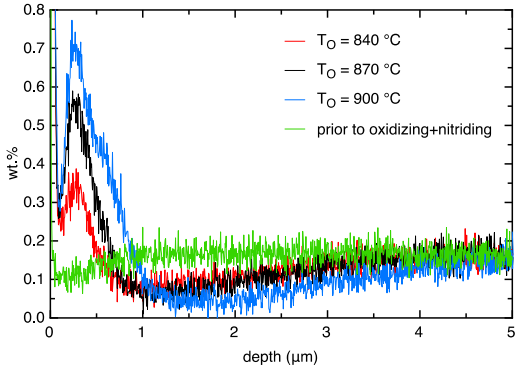

d. Manganese

Figure 7: GDOES chemical analyses of GO electrical steel. Influence of the oxidizing temperature (T_O) on (a) silicon, (b) chromium, (c) aluminium and (d) manganese in-depth content profiles.

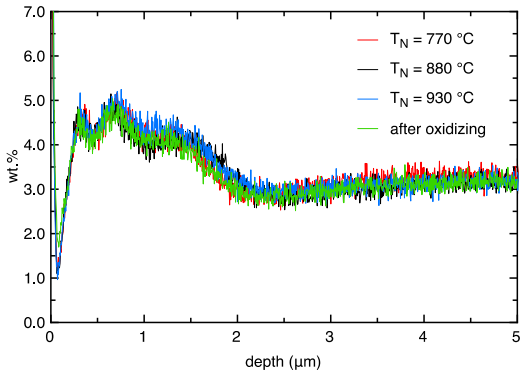

a. Silicon

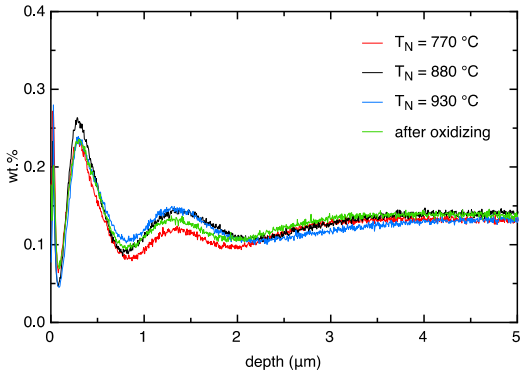

b. Chromium

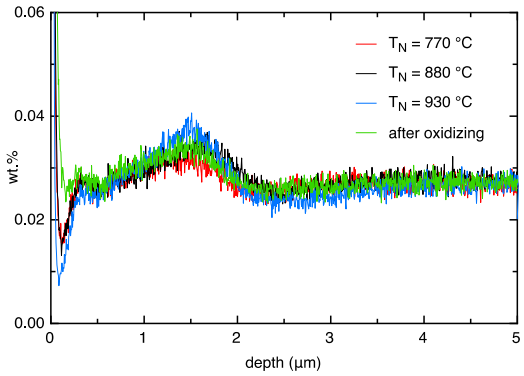

c. Aluminium

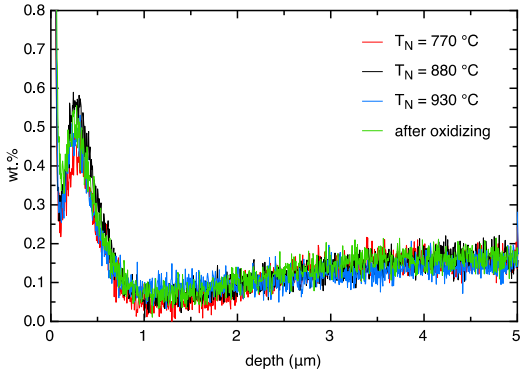

d. Manganese

Figure 8: GDOES chemical analyses of GO electrical steel. Influence of the nitriding temperature (T_N) on (a) silicon, (b) chromium, (c) aluminium and (d) manganese in-depth content profiles.

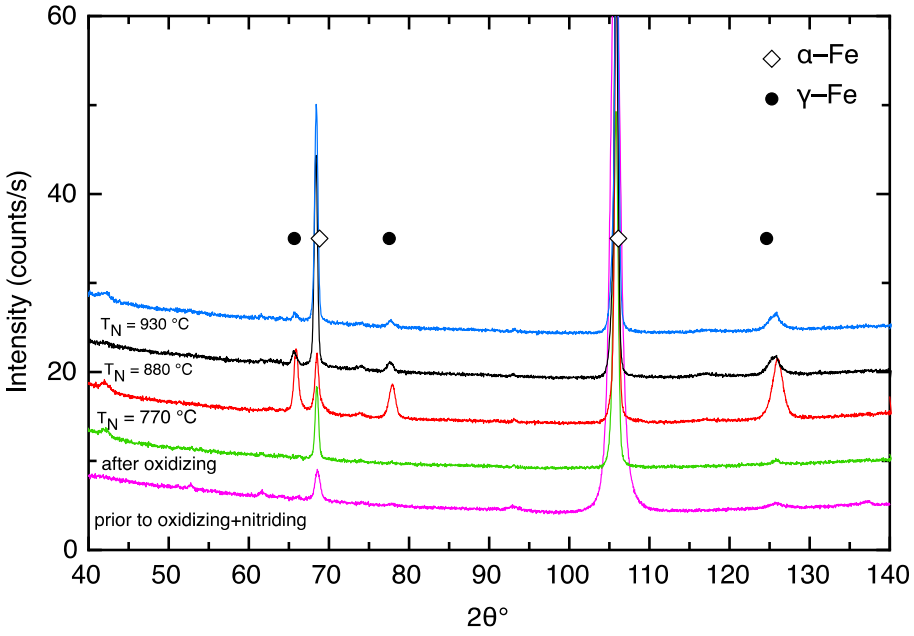

a. After nitriding

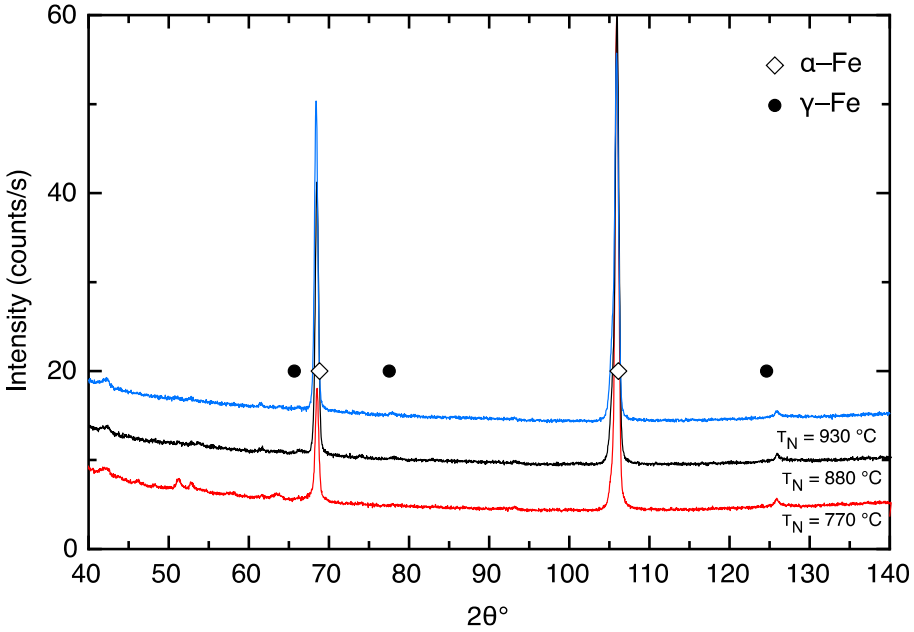

b. Tempering after nitriding

Figure 9: XRD phase analyses of GO electrical steel. Influence of the (a) nitriding temperature (T_N) and (b) tempering after nitriding.

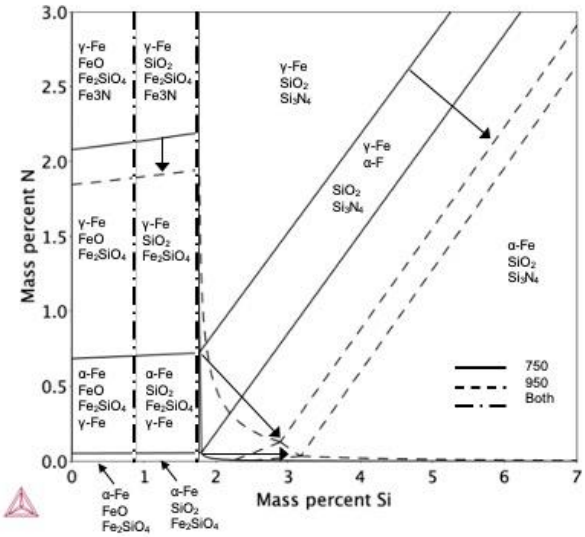

a.

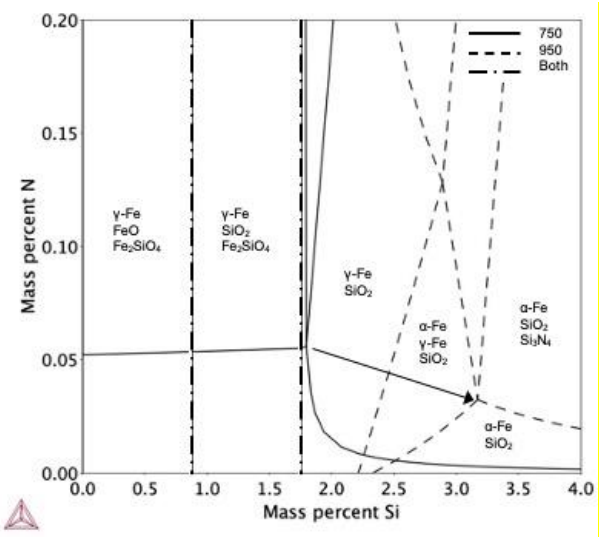

b.

Figure 10: Isopleth diagrams of Fe-Si-N-2.0wt.%O at 750 and 950 °C. (a) phase fields given for 750 °C. (b) phase fields given for 950 °C.

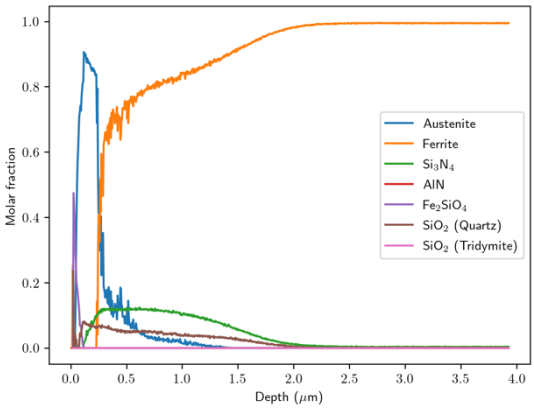

a. 770 °C

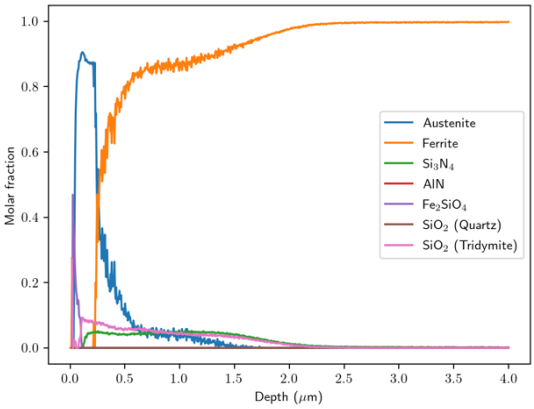

b. 880 °C

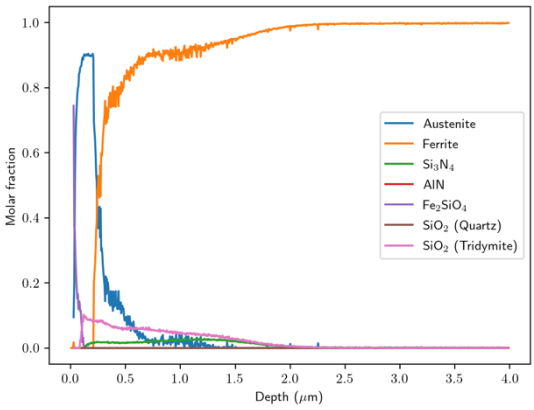

c. 930 °C

Figure 11: Calculations of the phase fractions as a function of the nitrogen content in an electrical steel according to GDOES analysis of the nitrided sample at (a) 770, (b) 880 and (c) 900 °C.